

Improvement of Ship Motion Control Using a Magnitude-Rate-Saturation Model

Ole Nikolai Lyngstadaas, Tore Egil Sæterdal, Mikkel Eske Nørgaard Sørensen, Morten Breivik

Abstract—Motion control concepts for ships have traditionally not been focused on handling actuator constraints. This paper aims to investigate the effects on performance of a pair of traditional control schemes by developing and implementing a magnitude-rate-saturation (MRS) model. The effects of the MRS model is tested in experiments with a model ship in an ocean basin. We also employ performance metrics to evaluate performance in terms of control error, energy consumption, and actuator wear and tear.

Index Terms—Ship motion control, Magnitude and rate saturation, Constraint handling, Nonlinear control, Model-scale experiments

I. INTRODUCTION

In traditional control theory, an ideal controller might achieve perfect reference tracking in simulation, having no or non-sufficient limitations on control input. It is not feasible in real life applications due to limitations in physical output and wear-and-tear of the actuators.

Several ways of handling actuator constraints have been investigated throughout the years. In [1], model predictive control for systems with actuator magnitude and rate constraints is presented. A state-of-the-art solution using a modified dynamic window approach to handle actuator constraints is investigated in [2], and further expanded in [3].

To easily include magnitude and rate saturation effects into a control system, a possible low-level approach to avoid saturation is to limit the output of the control signal within the limits of the actuators. However, this may lead to a underdamped, closed-loop system. To avoid this, effort has been put into implementing a model for combining magnitude and rate saturation (MRS) to smoothen control output within allowed hardware limits. In [4], an MRS model is derived to address the issue of anti-windup. The model used in this paper is based on the approach in [4].

The MRS effects, in this paper, are set at lower limits than the actual actuator constraints. The main purpose is to investigate how limiting the actuator's magnitude and rate outputs will impact the overall performance of the motion control system. The MRS model, depending on how it is tuned, can be implemented in a simulation scenario, where the purpose is to mimic the actual constraints of the system,

or be used to limit actuator outputs in laboratory experiments and aboard actual vessels.

The main contribution of this paper are the experimental results from scale testing on a 1:90 ship model. The MRS model from [4] is adapted to a three degree-of-freedom (DOF) ship model and tested under real conditions at the Marine Cybernetics Laboratory (MC-lab) at the Norwegian University of Science and Technology (NTNU) in Trondheim, Norway. Furthermore, the positive effects of employing MRS to a pair of nonlinear feedback control schemes from [5] have been investigated.

This paper is organized in five sections: Section II presents a mathematical model of a ship; Section III outlines assumptions and the control objective, derivation of the MRS model, and also presents a pair of nonlinear controllers from [5]; Section IV presents the experimental results from model-scale testing with discussion; while Section V concludes this paper.

II. SHIP MODEL

The motion of a ship can be represented by the pose vector $\eta = [x, y, \psi]^T \in \mathbb{R}^2 \times \mathbb{S}$ and the velocity vector $\nu = [u, v, r]^T \in \mathbb{R}^3$. Here, (x, y) represents the Cartesian position in the local earth-fixed reference frame, ψ is the yaw angle, (u, v) represents the body-fixed linear velocities and r is the yaw rate. The 3-DOF dynamics of a ship can then be stated as in [6]:

$$\dot{\eta} = R(\psi)\nu \quad (1)$$

$$M\dot{\nu} + C(\nu)\nu + D(\nu)\nu = \tau, \quad (2)$$

where $M \in \mathbb{R}^{3 \times 3}$, $C(\nu) \in \mathbb{R}^{3 \times 3}$, $D(\nu) \in \mathbb{R}^{3 \times 3}$ and $\tau = [\tau_1, \tau_2, \tau_3]^T$ represent the inertia matrix, Coriolis and centripetal matrix, damping matrix and control input vector, respectively. The rotation matrix $R(\psi) \in SO(3)$ is given by

$$R(\psi) = \begin{bmatrix} \cos(\psi) & -\sin(\psi) & 0 \\ \sin(\psi) & \cos(\psi) & 0 \\ 0 & 0 & 1 \end{bmatrix}. \quad (3)$$

The system matrices are assumed to satisfy the properties $M = M^T > 0$, $C(\nu) = -C(\nu)^T$ and $D(\nu) > 0$.

A. Nominal Model

The model and parameters of the model-scale ship C/S Inoceen Cat I Drillship [7], as shown in Fig. 1 and hereafter abbreviated CSAD, will be used throughout this paper. CSAD is a 1:90 scale replica of a supply ship, with a length of $L = 2.578$ m. The inertia matrix is given as

$$M = M_{RB} + M_A, \quad (4)$$

O. N. Lyngstadaas and T. E. Sæterdal are M.Sc. students at the Department of Engineering Cybernetics, Norwegian University of Science and Technology (NTNU), NO-7491 Trondheim, Norway. Email: {olenl,torees}@stud.ntnu.no. M. E. N. Sørensen and M. Breivik are with the Centre for Autonomous Marine Operations and Systems, Department of Engineering Cybernetics, Norwegian University of Science and Technology (NTNU), NO-7491 Trondheim, Norway. Email: {mikkel.e.n.sorensen, morten.breivik}@ieee.org

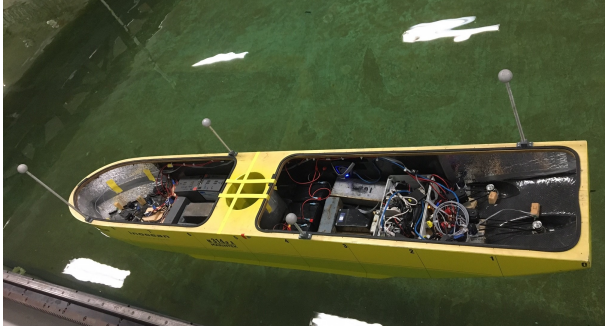


Fig. 1: C/S Inoceen Cat I Drillship in the MC-lab.

where

$$\mathbf{M}_{RB} = \begin{bmatrix} m & 0 & 0 \\ 0 & m & mx_g \\ 0 & mx_g & I_z \end{bmatrix} \quad (5)$$

$$\mathbf{M}_A = \begin{bmatrix} -X_{\dot{u}} & 0 & 0 \\ 0 & -Y_{\dot{v}} & -Y_{\dot{r}} \\ 0 & -N_{\dot{v}} & -N_{\dot{r}} \end{bmatrix}. \quad (6)$$

The mass of CSAD is $m = 127.92$ kg, while $x_g = 0.00375$ m is the distance along the x -axis in the body frame from the centre of gravity, and $I_z = 61.987$ kg m² is the the moment of inertia about the z -axis in the body frame. Other parameter values are listed in Table I, which are updated values from [7], where a few changes to the numerical values and signs has been done. The model was updated to fit the actual laboratory performance of CSAD.

CSAD has six azimuth thrusters, which in the experiments presented here are fixed to the angles $\delta = [\pi, \pi/4, -\pi/4, 0, 5\pi/4, 3\pi/4]$ in body-fixed coordinate system, giving a fully actuated vessel.

The Coriolis and centripetal matrix is

$$\mathbf{C}(\boldsymbol{\nu}) = \mathbf{C}_{RB}(\boldsymbol{\nu}) + \mathbf{C}_A(\boldsymbol{\nu}), \quad (7)$$

with

$$\mathbf{C}_{RB}(\boldsymbol{\nu}) = \begin{bmatrix} 0 & 0 & -m(x_g r + v) \\ 0 & 0 & mu \\ m(x_g r + v) & -mu & 0 \end{bmatrix} \quad (8)$$

$$\mathbf{C}_A(\boldsymbol{\nu}) = \begin{bmatrix} 0 & 0 & -c_{A,13}(\boldsymbol{\nu}) \\ 0 & 0 & c_{A,23}(\boldsymbol{\nu}) \\ c_{A,13}(\boldsymbol{\nu}) & -c_{A,23}(\boldsymbol{\nu}) & 0 \end{bmatrix}, \quad (9)$$

where

$$c_{A,13}(\boldsymbol{\nu}) = -Y_{\dot{r}}r - Y_{\dot{v}}v \quad (10)$$

$$c_{A,23}(\boldsymbol{\nu}) = -X_{\dot{u}}u. \quad (11)$$

Finally, the damping matrix $\mathbf{D}(\boldsymbol{\nu})$ is given as

$$\mathbf{D}(\boldsymbol{\nu}) = \mathbf{D}_L + \mathbf{D}_{NL}(\boldsymbol{\nu}), \quad (12)$$

where

$$\mathbf{D}_L = \begin{bmatrix} -X_u & 0 & 0 \\ 0 & -Y_v & -Y_r \\ 0 & -N_v & -N_r \end{bmatrix} \quad (13)$$

TABLE I: Parameters for CSAD, updated from [7].

Parameter	Value	Parameter	Value
$X_{\dot{u}}$	-3.262	$Y_{ r r}$	-3.450
$Y_{\dot{v}}$	-28.890	Y_{rrr}	0
$Y_{\dot{r}}$	-0.525	N_r	-6.916
$N_{\dot{v}}$	-0.157	$N_{ r r}$	-4.734
$N_{\dot{r}}$	-13.980	N_{rrr}	-0.147
X_u	-2.332	N_v	0
$X_{ u u}$	0	$N_{ v v}$	-0.209
X_{uuu}	-8.557	N_{vvv}	0
Y_v	-4.673	$N_{ r v}$	0.080
$Y_{ v v}$	-0.398	$N_{ v r}$	0.080
Y_{vvv}	313.300	$Y_{ r v}$	-0.805
Y_r	-7.250	$Y_{ v r}$	-0.845

$$\mathbf{D}_{NL}(\boldsymbol{\nu}) = \begin{bmatrix} d_{NL,11}(\boldsymbol{\nu}) & 0 & 0 \\ 0 & d_{NL,22}(\boldsymbol{\nu}) & d_{NL,23}(\boldsymbol{\nu}) \\ 0 & d_{NL,32}(\boldsymbol{\nu}) & d_{NL,33}(\boldsymbol{\nu}) \end{bmatrix}, \quad (14)$$

and

$$d_{NL,11}(\boldsymbol{\nu}) = -X_{|u|u}|u| - X_{uuu}u^2 \quad (15)$$

$$d_{NL,22}(\boldsymbol{\nu}) = -Y_{|v|v}|v| - Y_{|r|v}|v| - Y_{vvv}v^2 \quad (16)$$

$$d_{NL,23}(\boldsymbol{\nu}) = -Y_{|r|r}|r| - Y_{|v|r}|v| - Y_{rrr}r^2 - Y_{ur}u \quad (17)$$

$$d_{NL,32}(\boldsymbol{\nu}) = -N_{|v|v}|v| - N_{|r|v}|r| - N_{vvv}v^2 - N_{uv}u \quad (18)$$

$$d_{NL,33}(\boldsymbol{\nu}) = -N_{|r|r}|r| - N_{|v|r}|v| - N_{rrr}r^2 - N_{ur}u, \quad (19)$$

where

$$N_{ur} = Y_{\dot{r}} \quad (20)$$

$$N_{uv} = -(Y_{\dot{v}} - X_{\dot{u}}) \quad (21)$$

$$Y_{ur} = X_{\dot{u}}, \quad (22)$$

which are damping terms which are linearly increasing with the forward speed. This is added to compensate for the Munk moment and to get a more physically realistic model behavior [8].

III. CONTROL DESIGN

A. Control objective and four-corner test

The main control objective is to make $\tilde{\boldsymbol{\eta}}(t) \triangleq \boldsymbol{\eta}(t) - \boldsymbol{\eta}_t(t) \rightarrow \mathbf{0}$ when $t \rightarrow \infty$. For notational simplicity, time t will mostly be omitted for the rest of the paper.

It is desirable to investigate the effect of the magnetic rate-saturation model during different modes of ship motion. For this reason, a four-corner maneuvering test is used, as shown in Fig. 2. For comparison, the experiments will be conducted using both nominal control and the applied MRS-model to identify notable effects on performance.

The four-corner maneuvering test is proposed in [9] as a way to compare the performance of dynamic positioning control algorithms. The ship is first initialized in dynamic positioning to point straight North at heading 0 (deg). Then the following setpoint changes are commanded:

- Position change 2 (m) straight North: tests a pure surge movement ahead.

- Position change 2 (m) straight East: tests a pure sway movement in starboard direction.
- Heading change 45 (deg) clockwise: tests a pure yaw motion while keeping position steady.
- Position change 2 (m) straight South: tests a combined surge-sway movement while keeping heading steady.
- Position change 2 (m) straight West and heading change 45 (deg) counterclockwise: tests a combined surge-sway movement.

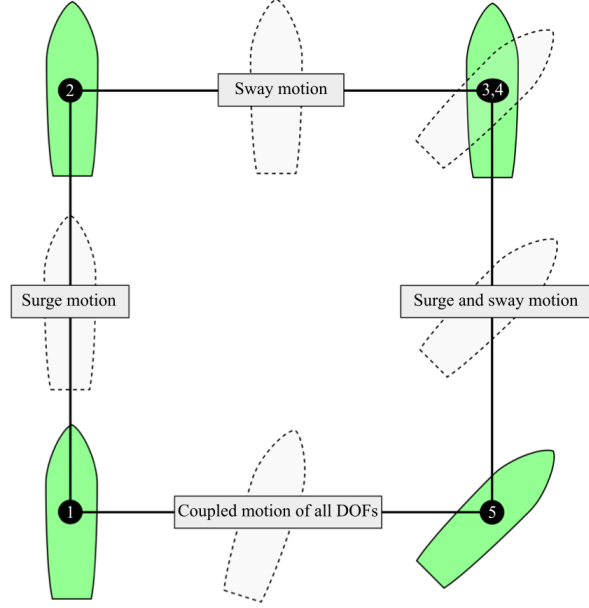


Fig. 2: The 4-corner dynamic positioning test. Modified from [9].

B. Magnitude-rate-saturation model design

Modelling the vessel's actuator constraints is important to ensure that the controller output remains inside a feasible value range. Both magnitude and rate constraints will impact a vessel's ability to maneuver, and should be handled in the control system.

1) *Saturation modeling*: A generalized saturation block for an actuator can be modeled as

$$\tau_{s,i}(\tau_i) = \begin{cases} \tau_{i,min} & \text{if } \tau_i \leq \tau_{i,min} \\ \tau_i & \text{if } \tau_{i,min} < \tau_i < \tau_{i,max}, \quad \forall i \in \{1, 2, 3\}, \\ \tau_{i,max} & \text{if } \tau_i \geq \tau_{i,max} \end{cases} \quad (23)$$

where τ_i is the commanded control input without saturation, and due to a 3-DOF ship model, $i \in \{1, 2, 3\}$ is to control surge, sway and yaw forces and moments, respectively. $\tau_{min} = [\tau_{1,min}, \tau_{2,min}, \tau_{3,min}]^T$ and $\tau_{max} = [\tau_{1,max}, \tau_{2,max}, \tau_{3,max}]^T$ with negative and positive bounded elements, respectively, represent the saturation limits.

2) *Magnitude-Rate Saturation model*: An approach to model the MRS effects is given by

$$\begin{aligned} \dot{\delta} &= \text{sat}_r(\dot{\tau}_c + K(\tau_c - \delta)) \\ \tau_{mrs} &= \text{sat}_m(\delta) \end{aligned} \quad (24)$$

where τ_c , δ and τ_{mrs} are the input, the state, and the output of the MRS model, respectively, and where $K > 0$ is a diagonal matrix and a free parameter ν is introduced in order to avoid an unstable cancellation between the derivative operator s in Fig. 3 and the integrator during linear operation, and thus $K \neq 1$. K affects the speed of the inner-loop in the MRS-model, and should be chosen based on the desired tracking performance. The derivative of the input, $\dot{\tau}_c$, is supposed to exist, and is calculated using numerical derivation. sat_r and sat_m are modeled as the saturation block above, and, respectively, contain the vessel's rate and magnitude constraints. See [4] for further details.

In this setup, the rate is limited first and the magnitude next, meaning that the state δ can exceed the magnitude bounds m , although the output τ_{mrs} never does. It should also be noted that this model can be further extended to effectively solve anti-windup problems, should such effects be needed to be accounted for.

The block diagram for the MRS model is shown in Fig. 3.

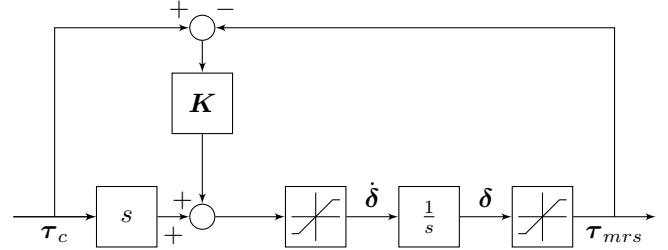


Fig. 3: Block diagram for the MRS model.

C. Nonlinear control design

The MRS model will be tested with two types of feedback controllers in order to test the impact on performance for both linear and nonlinear feedback terms.

1) *Nonlinear Pose and Linear Velocity Feedbacks*: Using a control scheme based on a combination of nonlinear feedback of pose and linear feedback of velocity from [5], the control input can be chosen as

$$\tau = M\dot{\alpha} + C(\nu)\alpha + D(\nu)\alpha - \Gamma_2 z_2, \quad (25)$$

where

$$\dot{\alpha} = R^T(\psi)\ddot{\eta}_t + S(r)^T R^T(\psi)\dot{\eta}_t - \dot{K}_1(\cdot)z_1 - K_1(\cdot)\dot{z}_1, \quad (26)$$

with $\Gamma_2 > 0$ and where

$$S(r) = \begin{bmatrix} 0 & -r & 0 \\ r & 0 & 0 \\ 0 & 0 & 0 \end{bmatrix}. \quad (27)$$

Here, the error variables $z_1 = [z_{1,x}, z_{1,y}, z_{1,\psi}]^T$ and $z_2 = [z_{2,u}, z_{2,v}, z_{2,r}]^T$ are defined as

$$z_1 \triangleq R(\psi)(\eta - \eta_t) \quad (28)$$

$$z_2 \triangleq \nu - \alpha, \quad (29)$$

where $\alpha \in \mathbb{R}^3$ is a vector of stabilizing functions, which can be interpreted as a desired velocity. As in [5], α can be chosen as

$$\alpha = R^\top(\psi)\dot{\eta}_t - K_1(\cdot)z_1, \quad (30)$$

with the nonlinear feedback term K_1 defined as

$$K_1(\cdot) = \Gamma_1 \begin{bmatrix} \frac{1}{\sqrt{z_{1,\bar{p}}^T z_{1,\bar{p}} + \Delta_{\bar{p}}^2}} I_{2 \times 2} & \mathbf{0}_{2 \times 1} \\ \mathbf{0}_{1 \times 2} & \frac{1}{\sqrt{z_{1,\bar{\psi}}^2 + \Delta_{\bar{\psi}}^2}} \end{bmatrix}, \quad (31)$$

with $z_{1,\bar{p}} = [z_{1,1}, z_{1,2}]^\top$, $z_{1,\bar{\psi}} = z_{1,3}$ and $\Delta_i > 0$ are tuning parameters.

2) *Nonlinear Pose and Velocity Feedbacks:* The other control scheme from [5] augments (25) with a nonlinear velocity feedback term, giving the control input

$$\tau = M\dot{\alpha} + C(\nu)\alpha + D(\nu)\alpha - K_2(\cdot)z_2, \quad (32)$$

where

$$\dot{\alpha} = R^\top(\psi)\ddot{\eta}_t + S(r)^\top R^\top(\psi)\dot{\eta}_t - \dot{K}_1(\cdot)z_1 - K_1(\cdot)\dot{z}_1, \quad (33)$$

with the feedback term $K_2(\cdot)$ defined as

$$K_2(\cdot) = \Gamma_2 \begin{bmatrix} \frac{1}{\sqrt{z_{2,\bar{\nu}}^T z_{2,\bar{\nu}} + \Delta_{\bar{\nu}}^2}} I_{2 \times 2} & \mathbf{0}_{2 \times 1} \\ \mathbf{0}_{1 \times 2} & \frac{1}{\sqrt{z_{2,\bar{\psi}}^2 + \Delta_{\bar{\psi}}^2}} \end{bmatrix}, \quad (34)$$

with $z_{2,\bar{\nu}} = [z_{2,1}, z_{2,2}]^\top$, $z_{2,\bar{\psi}} = z_{2,3}$ and $\Delta_i > 0$ are tuning parameters.

The nonlinear pose and velocity feedback controller will be abbreviated NP-NV, and nonlinear pose and linear velocity feedback NP-LV throughout this section.

3) *Stability:* Based on the theorems and stability proofs of [10], we can conclude that the two controllers have the following stability properties: The origin $(z_1, z_2) = (0, 0)$ is uniformly globally asymptotically stable (UGAS) and on each compact set $B \triangleq \{z_1, z_2\} \subset \mathbb{R}^6$ containing the origin, it is uniformly exponentially stable (UES) [10]. The MRS model is a nonlinear filter, and shown to not alter the stability property of the controller [4]. Thus, the cascaded system of feedback controller and MRS model as shown in Fig. 4 is proven to be stable.

4) *Parameter tuning:* The experiments are conducted with the gain parameters shown in Table II. The choice of the gain parameters for the two controllers are based the tuning rules described in [10]. Here, the goal is to make the kinetic subsystem faster than the kinematic subsystem, which means that the kinetic subsystem needs to have faster time constants than the kinematic subsystem in the linear region. The Δ -values scale the linear feedback gains and therefore the time constants of the linear region. The Δ -values must therefore be carefully chosen such that they do not make the kinematic subsystem faster than the kinetic subsystem.

The actuator saturation limits are chosen by following a set of suggested tuning rules as well [11]. Here, the magnitude saturation limits are set lower than the actual

limitations in order to save energy, and chosen as $\text{sat}_m = [2, 1.5, 1]$. The rate saturation limits are chosen by $r = [m_1/t_{MRS,1}, m_2/t_{MRS,2}, m_3/t_{MRS,3}]^\top$, where m_1, m_2 and m_3 are the magnitude saturation limits given by m , and where $t_{MRS,1}, t_{MRS,2}$ and $t_{MRS,3}$, are the desired transition time for the actuators to go from zero to max thrust in surge, sway and yaw, respectively. Here, suitable values for the rate saturation limits were found to be $\text{sat}_r = [1.9, 1.1, 0.8]$. Then, the gain matrix K can be chosen by $K = \text{diag}([K_1, \frac{m_2}{m_1} K_1, \frac{m_3}{m_1} K_1])$, where, under normal operations, it is desired to have the lowest value of $K > 1$. Here, $K_1 = 4$ to ensure a fast tracking of the target signal in all 3 degrees-of-freedom. The block diagram for the full control system is shown in Fig. 4.

TABLE II: Control gains.

	NP-LV	NP-NV
Γ_1	$\text{diag}([0.08, 0.08, 0.0698])$	— —
Γ_2	$\text{diag}([0.2, 0.2, 0.1745])M$	— —
$\Delta_{\bar{p}}$	0.5	— —
$\Delta_{\bar{\psi}}$	0.5	— —
$\Delta_{\bar{\nu}}$	—	0.7
$\Delta_{\bar{\psi}}$	—	1
K	$\text{diag}([4, 3, 2])$	— —

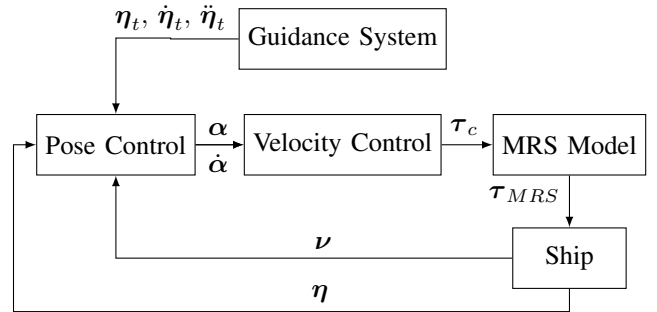


Fig. 4: Block diagram for the ship control system.

IV. EXPERIMENTAL RESULTS AND PERFORMANCE EVALUATION

A. Marine Cybernetics Laboratory

As mentioned earlier, the Marine Cybernetics laboratory (MC-lab) is a small ocean basin operated by the Department of Marine Technology at NTNU. Due to its relatively small size and advanced instrumentation package, the facility is especially suited for tests of motion control system for marine vessels, but is also suitable for more specialized hydrodynamic tests due to the advanced towing carriage, which has capability for precise movement of models up to six degrees-of-freedom [12].

The experiments will be conducted under the following conditions: The Coriolis and centripetal and damping matrices, C and D , respectively, as well as the thrust allocation for the CSAD, have inherent uncertainties, which can be interpreted as disturbances in the control system.

Furthermore, measurement noise is assumed present in the Qualisys motion tracking system used in the lab.

B. Performance metrics

Performance metrics are a commonly used method to compare performance of different control schemes. The analysis of these metrics is challenging, as the response differs depending on what type of performance is being analyzed. In this paper, the error variable is defined as the scaled norm of the pose control error z_1

$$e = \sqrt{\bar{z}_1^\top \bar{z}_1}. \quad (35)$$

Since the position and yaw angle in pose have different units, we define the normalized pose error signals $\bar{z}_{1,x}$, $\bar{z}_{1,y}$ and $\bar{z}_{1,\psi}$ on the intervals $[-0.5, 0.5]$ in the expected operational space of the ship [13]. To get this interval, the position errors are divided by 4 and the yaw error is divided by $\frac{\pi}{2}$, since the position errors are in the intervals $[-2, 2]$ and the yaw error is in the interval $[-\frac{\pi}{4}, \frac{\pi}{4}]$, resulting in the scaled pose control error

$$\bar{z}_1 = \left[\frac{z_{1,x}}{4}, \frac{z_{1,y}}{4}, \frac{z_{1,\psi}}{\pi/2} \right]^\top. \quad (36)$$

Three different performance metrics are used to evaluate the MRS in this paper; IAE, IAEW and IADC.

The IAE (integral of the absolute error) metric is defined as an unweighted integral over time:

$$IAE(t) = \int_0^t |e(\gamma)| d\gamma. \quad (37)$$

The IAEW (integral of the absolute error multiplied by energy consumption) takes the energy into account, using $P = \|\nu^\top \tau\|$ in a double integral:

$$IAEW(t) = \int_0^t |e(\gamma)| d\gamma \int_0^t P(\gamma) d\gamma. \quad (38)$$

Since the aim of the MRS-model is also to reduce actuator wear-and-tear, it is interesting to investigate the rate of the control signal. The IADC (integral of absolute differentiated control) metric is defined as in [13]:

$$IADC(t) = \int_{t_0}^t |\dot{\bar{\tau}}(\gamma)| d\gamma, \quad (39)$$

with $\bar{\tau}(t) = \sqrt{\tau^\top \tau}$, and where the variable $\dot{\bar{\tau}}$ is computed using numerical derivation.

C. Experimental results

While the CSAD has a length of $L = 2.578m$, it has been further scaled by 1:6 in the 4-corner plots in Fig. 5 and 8, to better display the ship behaviour.

By the plotted values of the performance metrics in Fig. 6 and 9, the effects of the MRS-model on control performance can be examined.

Fig. 5 displays guidance trajectory and actual trajectory for the CSAD with and without the MRS-model applied to the

TABLE III: Performance metrics.

	NP-LV	NP-LV MRS	NP-NV	NP-NV MRS
IAE final	93	93	89	90
IAEW final	410	381	461	404
IADC final	96	58	119	64

NP-LV control. The results show no remarkable difference in the trajectory.

The performance metrics are plotted in Fig. 6. The metrics show that the while MRS does not reduce the overall tracking error by the IAE metric, both energy consumption (IAEW) and actuator wear-and-tear (IADC) are reduced by 7% and 39%, respectively.

In Fig. 7, the commanded thrust signals are shown for the 4-corner test. It can be seen that the MRS contributes to a smoother and amplitude-wise smaller control signal, while achieving approximately the same tracking performance. The spikes that can be seen in the control signal, especially during transients, are caused by noise in the velocity estimation.

Fig. 8 displays the 4-corner trajectory for the NP-NV controller. Even though the NP-NV controlled vessel with MRS effects takes a wider arch in the coupled motion ($5 \rightarrow 1$) in Fig. 2, the overall tracking error is not increased, as seen in Table III.

Furthermore, Fig. 9 shows improvement in energy efficiency, shown by the IAEW metric, and lower actuator wear-and-tear by reduced control rate in the IADC metric. The reduction is greater for the NP-NV controller than the NP-LV, which is due to the fact that the NP-NV is inherently a more aggressive control scheme, and thus benefits more from the fitting of a MRS-model. For the NP-NV, the reduction is 12% and 46% for IAEW and IADC, respectively.

Fig. 10 shows the commanded control inputs for the NP-NV controller. As for the NP-LV, a smoothing effect can be observed, although less significant than the former. This is likely due to the nature of the pure nonlinear feedback, giving overall better tracking performance, which has previously been discussed in [5].

A significant effect of the MRS model, which can be seen in the performance metrics in Fig. 6 and 9, is that the MRS model leads to a significantly reduced rate of change in the commanded control input.

The final values for the performance metrics are displayed in Table III, where the best results are noted in bold. The metric values are rounded to the nearest integer for readability.

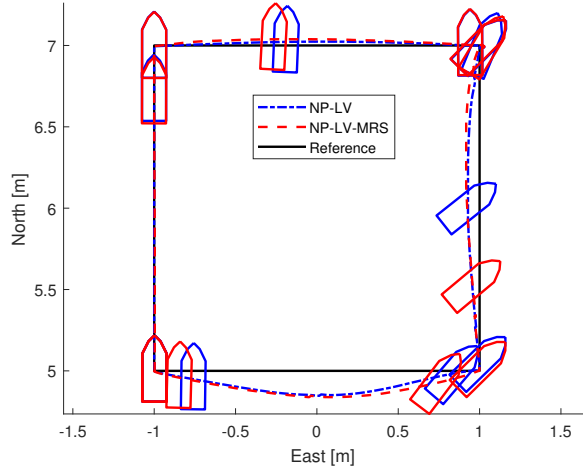


Fig. 5: Vessel performing the 4-corner manoeuvre using the NP-LV controller.

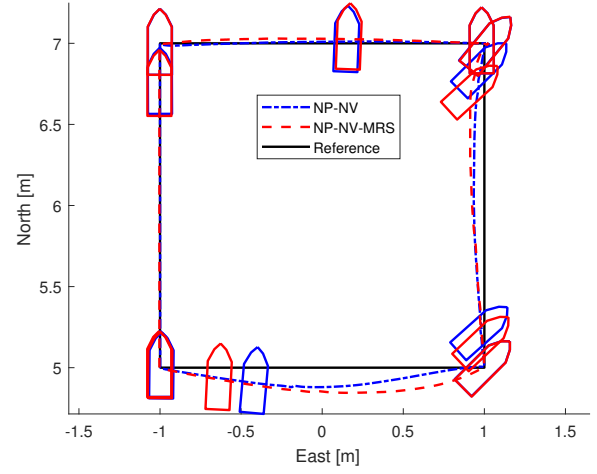


Fig. 8: Vessel performing the 4-corner manoeuvre using the NP-NV controller.

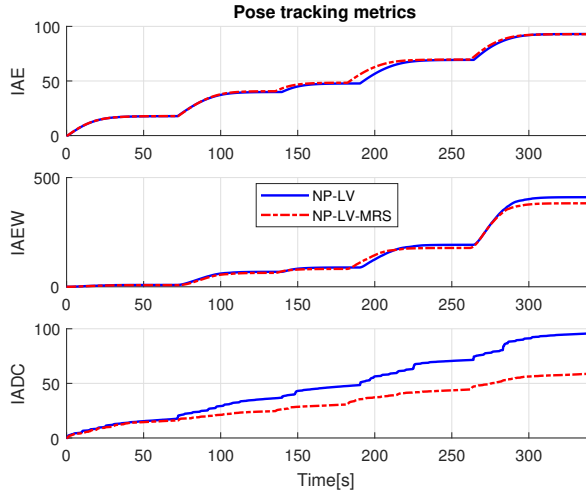


Fig. 6: Performance metrics for NP-LV.

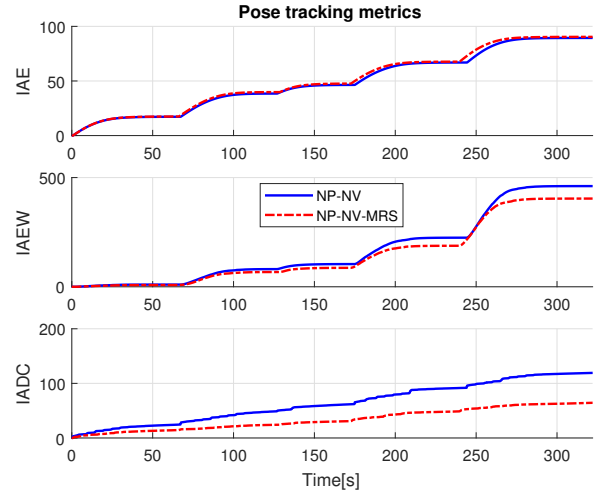


Fig. 9: Performance metrics for NP-NV.

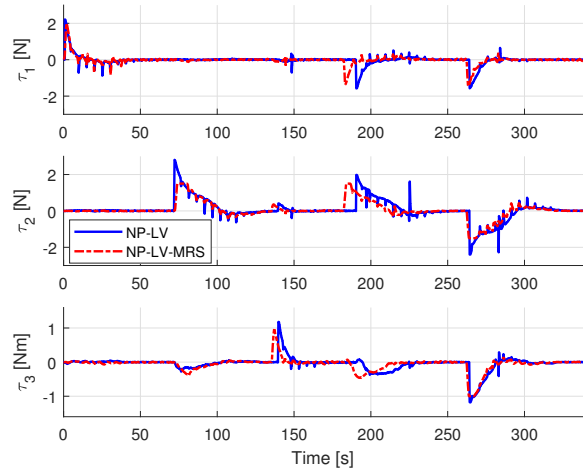


Fig. 7: Commanded control input for NP-LV.

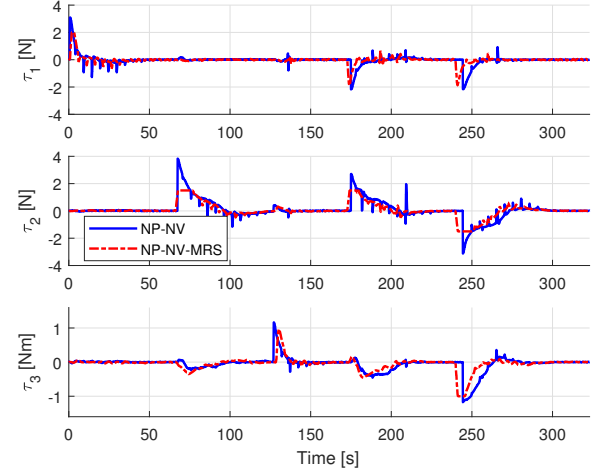


Fig. 10: Commanded control input for NP-NV.

V. CONCLUSION


Depending on the type of controller that is being used, including a MRS module to limit actuator magnitude and rate output can contribute positively in several ways. As seen in both cases presented, an MRS model can efficiently reduce actuator twitching, and thus wear-and-tear, without the degradation of performance in vessel control. In addition, it has potential to improve overall energy efficiency and pose tracking abilities, as can be seen from the performance metrics and path following plots, and can have positive effects on ship performance in set-point navigation. These effects are especially important for vessels which must operate for longer times at sea, and can deem notably useful for ships in DP operations, thus contributing to the longevity of the operation and less time and money spent on maintenance and repairs.

Future works include optimizing the MRS module to further improve performance. This includes, through experimental tests in a laboratory, further tuning of the gain parameter K and the desired magnitude and rate saturation effects to obtain optimal ship control for the wanted ship operational environment.

ACKNOWLEDGEMENTS

This work was supported by the Research Council of Norway through the Centres of Excellence funding scheme, project number 223254. The authors gratefully acknowledge senior engineer Torgeir Wahl and Ph.D. candidate Andreas R. Dahl at NTNU's Department of Marine Technology for valuable support during the experiments.

REFERENCES

- [1] V. Kapila and S. Valluri, "Model predictive control of systems with actuator amplitude and rate saturation," in *Proceedings of the 37th IEEE Conference on Decision and Control*, pp. 1396-1401, 1998.
- [2] M. E. N. Sørensen, M. Breivik, and B. O. H. Eriksen, "A ship heading and speed control concept inherently satisfying actuator constraints," in *Proceedings of the 1st IEEE Conference on Control Technology and Applications, HI, USA*, 2017.
- [3] M. E. N. Sørensen, O. N. Lyngstadaas, and M. Eriksen, B. O. H. Breivik, "A dynamic window-based controller for dynamic positioning satisfying actuator constraints," in *Proceedings of the 11th IFAC Conference on Control Applications in Marine Systems, Robotics, and Vehicles, Opatija, Croatia*, 2018.
- [4] S. Galeani, S. Onori, A. R. Teel, and L. Zaccarian, "A magnitude and rate saturation model and its use in the solution of a static anti-windup problem," *Systems & Control Letters*, Volume 57, Issue 1, pp. 1-9, 2008.
- [5] M. E. N. Sørensen and M. Breivik, "Comparing combinations of linear and nonlinear feedback terms for motion control of marine surface vessels," in *Proceedings of the 10th IFAC Conference on Control Applications in Marine Systems, Trondheim, Norway*, 2016.
- [6] T. I. Fossen, *Handbook of Marine Craft Hydrodynamics and Motion Control*. Wiley, 2011.
- [7] J. Bjørnø, *Thruster-Assisted Position Mooring of C/S Inocean Cat I Drillship*. Master thesis, Norwegian University of Science and Technology, Trondheim, Norway, 2016.
- [8] J. E. Refsnes, *Nonlinear Model-Based Control of Slender Body AUVs*. PhD thesis, Department of Marine Technology, Norwegian University of Science and Technology, Trondheim, Norway, 2008.
- [9] R. Skjetne, M. E. N. Sørensen, M. Breivik, S. A. T. Værnø, A. H. Brodtkorb, A. J. Sørensen, Ø. K. Kjerstad, V. Calabrò, and B. O. Vinje, "AMOS DP research cruise 2016: Academic full-scale testing of experimental dynamic positioning control algorithms onboard R/V Gunnerus," in *Proceedings of the 36th International Conference on Ocean, Offshore and Arctic Engineering*, vol.  Offshore Technology, 2017.
- [10] M. E. N. Sørensen, M. Breivik, and R. Skjetne, "Comparing combinations of linear and nonlinear feedback terms for ship motion control," submitted to *IEEE Transactions on Control Systems Technology*, 2018.
- [11] O. N. Lyngstadaas, *A Ship Motion Control Concept Inherently Satisfying Actuator Constraints*. Master thesis, Department of Engineering Cybernetics, Norwegian University of Science and Technology, Trondheim, Norway, 2018.
- [12] "Marine cybernetics laboratory." <https://www.ntnu.edu/imt/lab/cybernetics>. Accessed: 2018-01-30.
- [13] B.-O. H. Eriksen and M. Breivik, *Modeling, Identification and Control of High-Speed ASVs: Theory and Experiments*, pp. 407-431. Sensing and Control for Autonomous Vehicles: Applications to Land, Water and Air Vehicles, Springer International Publishing, 2017.